THE JOURNAL OF PHYSICAL CHEMISTRY Letters

Letter

pubs.acs.org/JPCL

Kinetics of Oxygen Reduction in Aprotic Li–O_2 Cells: A Model-Based Study

M. Safari, B. D. Adams, and L. F. Nazar*

Department of Chemistry, University of Waterloo, 200 University Avenue West, Waterloo, Ontario N2L 3G1, Canada

ABSTRACT: A comprehensive and general kinetic model is developed for the oxygen reduction reaction in aprotic Li–O_2 cells. The model is based on the competitive uptake of lithium superoxide by the surface and solution. A demonstrative kinetic study is provided to demystify the origin of curvature in Tafel plots as well as the current dependency and aberrant diversity of the nature and morphology of discharge products in these systems. Our results are general and extend to any system where solubilization of superoxide is favored, such as where phase-transfer catalysts play an important role.

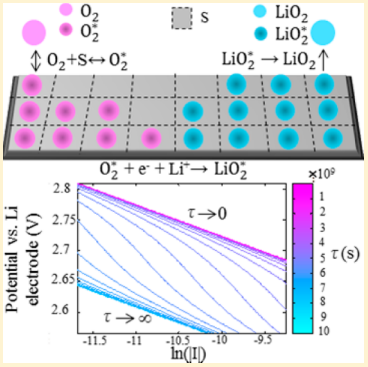

SECTION: Energy Conversion and Storage; Energy and Charge Transport

Lithium-air batteries have the potential to propel electric vehicles into the mainstream. These batteries benefit from substantially larger theoretical specific capacities compared to lithium-ion batteries, but they are still in early stages of development.[1] Before their practical realization, there are many obstacles to overcome such as poor rechargability,[2] rate-capability,[3] and cycle life.[4] These issues are linked together to a great extent and share a fundamental origin, which is the sensitive kinetics of oxygen reduction (ORR) and evolution (OER) reactions in aprotic media.[5−8] Hence, the fundamental study of kinetics at the oxygen electrode in these systems is of prime importance. Contrary to the case of aqueous media,[9,10] there are a limited number of studies that investigate the electrochemical kinetics of oxygen electrodes in aprotic electrolytes. The yet unresolved debate among researchers concerning the detailed mechanism of ORR and discharge intermediates/products clearly demonstrates the complex nature of interactions in these systems.[11−16]

With respect to the ORR in aprotic electrolytes, a careful examination reveals that the interplay between the surface and solution-phase intermediates can explain the diversity in the reported overpotentials as well as nature and morphology of the discharge products.[17,18] The list of experimental clues that support this claim include, but are not limited to, reports of an oxygen-rich superoxide-like component (LiO_2) in the final discharge product,[19−21] lower discharge overpotentials observed in water-contaminated cells,[22] the current/voltage-dependent morphology of discharge products,[19,23,24] and curvature in Tafel plots.[25] To date, in spite of the various pathways proposed for the ORR in aprotic electrolytes, there is no report of a model-based study in which the contributions from both the surface[7,15,25] and solution species are quantitatively elucidated. A recent study used a continuum model based on a theory of electrochemical nonequilibrium thermodynamics to probe the dynamics of Li_2O_2 growth but did not address the actual kinetic steps that underlie the mechanism of its formation.[26] Here, for the first time, we present such a study in which a simple but holistic kinetic model is developed to shed light on the above listed critical factors during ORR in aprotic electrolytes.

Our focus is on the main kinetic steps, recognizing that a comprehensive portrait of the ORR kinetics in aprotic Li–O_2 cells is complicated by the specific nature of cathode/electrolyte interactions[11,12,27,28] and the resistive characteristics of the discharge (by)products.[29,30] The system dynamics is neglected and the model only addresses the steady-state behavior. This is especially a valid assumption in the case of carbon-based cathodes where the potential rapidly levels off toward a plateau over a wide range of current densities. We note that the transport of reactants (i.e., oxygen, Li^+ ions) will not result in tangible gradients in the solution phase, based on the practical currents used in the study of these systems.[30]

The adsorption of oxygen on the surface free/active sites (S) (eq 1) can reasonably be treated as an equilibrated process with respect to the other chemical/electrochemical steps involved in the ORR

$$O_2 + S \leftrightarrow O_2^* \quad (1)$$

In eq 1, S represents the free/active surface sites and * denotes the adsorbed state. The following equation (eq 2) relates the

Received: August 28, 2014
Accepted: September 19, 2014
Published: September 22, 2014

   dx.doi.org/10.1021/jz5018202 | J. Phys. Chem. Lett. 2014, 5, 3486−3491

fraction of surface covered by the ad-oxygen (θ_{O_2}) and free sites (θ_S)

$$\theta_{O_2} = \frac{k_a c_{O_2}}{k_d}\theta_s = w\theta_s \tag{2}$$

where, c_{O_2} (mol m^{-3}) stands for the oxygen concentration in solution adjacent to the electrode surface and k_a (m^3 s^{-1} mol^{-1}) and k_d (s^{-1}) are the adsorption and desorption rate constants, respectively. Hereafter, w (dimensionless) replaces the three constants in eq 2.

The formation of the lithium superoxide (eq 3) is regarded as the first electrochemical step in ORR in aprotic electrolytes. The succeeding predominant pathways are derived either from the further electrochemical reduction of lithium superoxide (eq 4) or their chemical disproportionation via a solution phase (eq 5) or a surface route (eq 6) that forms lithium peroxide[12−14]

$$O_2^* + e^- + Li^+ \rightarrow LiO_2^* \tag{3}$$

$$LiO_2^* + e^- + Li^+ \rightarrow Li_2O_2^* \tag{4}$$

$$LiO_2 + LiO_2 \rightarrow Li_2O_2 + O_2 \tag{5}$$

$$LiO_2^* + LiO_2^* \rightarrow Li_2O_2^* + O_2^* \tag{6}$$

Given reactions 3 and 4, which are strongly driven to the right in a Li−O_2 cell during ORR, it is valid to neglect the backward (anodic) reactions in eqs 3 and 4.[31] By doing so and in the abundance of Li^+, the following kinetic equations describe the rate of electrochemical reduction of ad-oxygen to ad-lithium-superoxide (r_1) (eq 7) and ad-lithium-superoxide to ad-lithium-peroxide (r_2) (eq 8):

$$-r_1 = \frac{I_1}{FA} = -k_{c1}\Gamma\theta_{O_2}\exp\left(-\frac{\beta_1 F}{RT}\Phi\right) \tag{7}$$

$$-r_2 = \frac{I_2}{FA} = -k_{c2}\Gamma\theta_{LiO_2}\exp\left(-\frac{\beta_2 F}{RT}\Phi\right) \tag{8}$$

where Φ (V) is the electrode potential with respect to a reference electrode (e.g., lithium); Γ is the maximum surface-site concentration (mol m^{-2}); k_{c1} (s^{-1}), and k_{c2}(s^{-1}) are the rate constants; β_1 and β_2 are the charge transfer symmetry factors; and I_1 and I_2 are the current flows (A) in the reduction of ad-oxygen and ad-lithium-superoxide, respectively. The term A (m^2) is the total active area of the electrode, and T (K), R (J mol^{-1} K^{-1}), and F (C mol^{-1}) have their usual meaning.

A finite lifetime for the lithium superoxide not only can increase the chance of its engagement in the chemical disproportionation reaction[13,19,21] but also can enhance side reactions with electrolyte initiated by these highly reactive nucleophiles.[27,32,33] Disproportionation or side reaction notwithstanding, the competitive uptake of lithium superoxide by the surface and solution-mediated reactions should certainly be a part of any realistic kinetic picture for this system. Our kinetic model does not explicitly account for the details of these reactions. Instead, we only allow the surface overflow of lithium superoxide—as a result of a kinetic mismatch between the rates of ad-lithium-superoxide formation (eq 3) and consumption (eq 4)—toward the solution phase reactions (i.e., disproportionation or side reactions).[31] A mass balance on LiO_2^* is expressed as

$$\Gamma\frac{\partial\theta_{LiO_2}}{\partial t} = r_1 - r_2 - r_s \tag{9}$$

where r_s represents the consumption rate of LiO_2^* due to solution-mediated reactions and can be approximated with a first-order dependence on LiO_2^*, that is,

$$r_s = k_s\Gamma\theta_{LiO_2} \tag{10}$$

where k_s is an effective rate constant of the hypothetical solution-mediated reactions. It (k_s) can be represented as $1/\tau$, where τ is a characteristic time constant for the LiO_2^* removal from surface via solution-mediated reactions (i.e., desorption time constant). Upon rearrangement of eqs 7−10 and under steady-state conditions (i.e., $(\partial\theta_{LiO_2}/\partial t) = 0$), the following equation equates the surface overflow of lithium superoxide to their rate of consumption in the solution-mediated reactions

$$\frac{(I_2 - I_1)}{FA} = \frac{\Gamma}{\tau}\theta_{LiO_2} \tag{11}$$

In the present treatment, surface disproportionation (eq 6) has been neglected with respect to the solution phase (eq 5). Although some theoretical studies have suggested low barriers to disproportionation, others have concluded that higher barriers exist, for example, in the case of large LiO_2 cluster formation.[18] The nature of the surface will also play a role, as LiO_2 will be much less mobile on some cathode supports than on others. Moreover, on cell discharge, experimental discrimination between a sequential charge transfer process (eq 4) (that we do take into account) and a very fast surface disproportionation reaction (eq 6) is very challenging.[15] As this has not yet been accomplished, even approximate rate constants for surface disproportionation are unavailable. Nonetheless, the preponderance of large toroidal/plate crystalline Li_2O_2 aggregates in the Li−O_2 battery literature—which can only arise from nucleation in solution—suggests that a much faster consumption rate of LiO_2* due to solution-mediated reactions is a valid assumption, especially for intermediate and even fast[34] current rates.

Figure 1 summarizes the main steps involved in ORR in the view of the present model. Finally, expressions for the balance

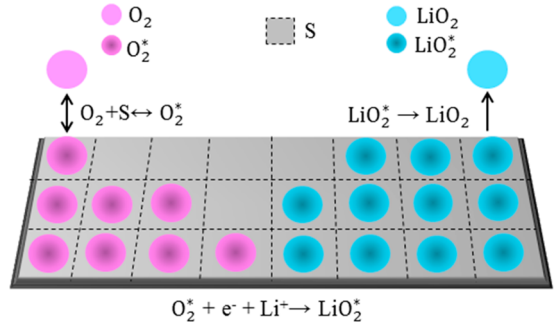

Figure 1. Schematic of the main steps accounted for in the kinetic model proposed in this study for the ORR.

of total current (eq 12) and surface-site population (eq 13) complete the list of equations used in the model

$$I = I_1 + I_2 \tag{12}$$

$$\theta_{O_2} + \theta_{LiO_2} + \theta_s = 1 \tag{13}$$

dx.doi.org/10.1021/jz5018202 | J. Phys. Chem. Lett. 2014, 5, 3486−3491

Table 1. Values for the Set of Parameters Used in This Study for the Kinetic Simulations

parameter	k_{c1} (s^{-1})	k_{c2} (s^{-1})	β	w	A.Γ (mol)	τ (s)	T (K)	R (J mol^{-1} K^{-1})	F (C mol^{-1})
value	10^{19}	10^{17}	0.5	1	10^{-5}	10^{-4}–10^{10}	298	8.314	96485

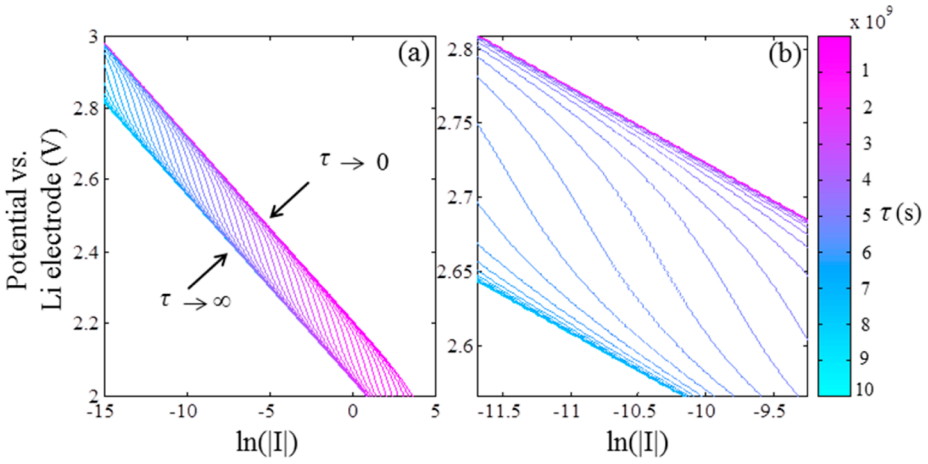

Figure 2. Tafel-plot simulations for ORR using parameters listed in Table 1(a) over a potential range of 2 and 3 V and τ between 10^{-4} (magenta) and 10^{10} (blue); (b) expanded region of panel a over the potential range of 2.5 and 2.81 V.

In our physical picture, we assume that any peroxide on the surface will act as an active substrate (i.e., free site or θ_s) for continued adsorption of oxygen. Equivalent to surface electrochemical growth, this is valid in the early stages where electronic limitations are negligible.

Thus, there are six equations (eq 2, eqs 7−8, and 11−13) necessary for an unequivocal solution of six unknowns, that is, θ_s, θ_{O_2}, θ_{LiO_2}, I_1, I_2, Φ. After algebraic manipulation, the total current (I) is expressed as a function of potential (Φ)

$$-\frac{I}{FA\Gamma} = k_{c1} w \theta_s \exp\left(-\frac{\beta_1 F}{RT}\Phi\right) + k_{c2}(1 - (1 + w)\theta_s) \exp\left(-\frac{\beta_2 F}{RT}\Phi\right) \quad (14)$$

where θ_s is

$$\theta_s = \frac{1}{(1 + w)} + \frac{I}{2\Gamma FA(1 + w)\left[k_{c2}\exp\left(-\frac{\beta_2 F}{RT}\Phi\right) + \frac{1}{2\tau}\right]} \quad (15)$$

If we further simplify the analysis and take the charge transfer symmetry factors to be equivalent, (i.e., $\beta_1 = \beta_2 = \beta$), which is a very reasonable approximation, the overall current can be expressed as

$$-\frac{I}{FA\Gamma} = \frac{k_{c1} w \exp\left(-\frac{\beta F}{RT}\Phi\right)}{\left(\frac{1}{(1 + w)} + \frac{(k_{c1} - k_{c2})w - k_{c2}}{2(1 + w)^2\left[k_{c2}\exp\left(-\frac{\beta F}{RT}\Phi\right) + \frac{1}{2\tau_s}\right]}\exp\left(-\frac{\beta F}{RT}\Phi\right)\right)} \quad (16)$$

Note that Φ in eq 16 can be replaced by an overpotential ($\eta = \Phi - \Phi_{eq}$) if an equilibrium potential (Φ_{eq}) can be defined. However, the irreversible nature of the ORR in the presence of impurities prevents one from a successful measurement of equilibrium oxygen potential. Instead, one can use an open-circuit potential, which is not an equilibrium potential but a mixed potential.[31] Thus, in the following analysis, we use Φ rather than an explicit overpotential, where the rate constants are linked to the potential.

At room temperature and atmospheric pressure, seven parameters, that is, k_{c1}, k_{c2}, w, τ, Γ, A, and β should be given set values in eq 16 in order to visualize a polarographic plot. These parameters are very system specific and sensitive largely to the cathode material and electrolyte composition. The value of the parameters (Table 1) have been adjusted so that a qualitative match is obtained with the I−Φ range found in the literature for ORR in aprotic Li−O_2 cells. Moreover, here, the analysis is limited to underscore the crucial impact of reaction-zone distribution between the surface and solution phase, although a sensitivity analysis of model parameters is of equal interest.

Tafel plots are widely used to discuss the experimental I−Φ trends in electrochemical kinetic studies, where—for sufficiently large deviations from equilibrium—a linear correlation between the potential and logarithm of current is usually observed for noncatalytic, simple, and single step reduction/oxidation.[31,35] The experimental Tafel plots reported for ORR in Li−O_2 aprotic cells feature significant curvature regardless of the cell conditions, as also reported elsewhere.[25] In ref 25, this curvature was ascribed to the potential-dependent energy of nonstoichiometric O-rich surfaces of lithium peroxide. Figure 2 presents the simulated Tafel plots for a wide range of τ. In Figure 2a and b, τ has been color-coded from blue for a very large desorption time constant (10^{10} s), to magenta for sufficiently small τ (10^{-4} s). A linear trend is obtained over the full range of potential (current) for extreme values of τ, or when the kinetic mismatch between the first and second reduction (eq 3 and 4) is negligible. For the intermediate values of τ, however, Tafel plots exhibit two linear branches over the outermost potential (current) ranges and a curved region in the middle (Figure 2b). The domain of potential (current) where the Tafel plot experiences curvature depends on τ. It descends from higher potential ranges for a large desorption time constant to lower ranges for small values of τ. Figure 2 clearly

dx.doi.org/10.1021/jz5018202 | J. Phys. Chem. Lett. 2014, 5, 3486−3491

shows that the curvature in the Tafel plot originates from a finite kinetic mismatch between reduction of ad-oxygen and ad-lithium-superoxide ($I_2 \neq I_1$). The kinetic mismatch alone and without a finite delocalization (i.e., finite τ) of lithium superoxide from the surface is not enough to induce the curvature in the Tafel plot. Hence, the experimental reports on the curvature necessarily imply the contribution of reactions in solution (i.e., chemical disproportionation or side reactions). This is completely in line with the reports of LiO_2 like species detected as an intermediate during ORR, along with the final discharge products being comprised of superoxide-enriched Li_2O_2 as well as carbonates.[19−21]

In Figure 2, the simulation results suggest that at a given current, higher discharge potentials are obtained for smaller values of τ (Figure 2a and b). This finding is best illustrated in Figure 3. In this Figure, each contour line belongs to a constant

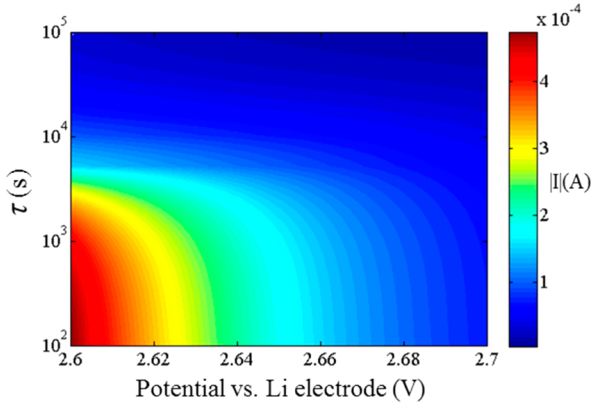

Figure 3. Simulated contour plots of discharge current in a plane defined by potential as x axis and τ as the y axis. The parameters used in the simulation are listed in Table1. The current has been color-coded for clarity.

discharge current and the current values have been color-coded for better resolution, that is, from blue for small currents to red for higher currents. Figure 3 clearly shows that desorption of lithium superoxide from the surface and its engagement in solution reactions, that is, chemical disproportionation or side reactions can improve the apparent ORR kinetics. In the case of the latter, the higher discharge potential could be erroneously interpreted as better battery performance. On account of side reactions — that are extremely difficult to avoid in ORR in aprotic Li−O_2 cells — enhanced desorption of lithium superoxide from the surface can explain the higher discharge potentials reported for water−vapor contaminated cells.[22] Moreover, our findings support the results of a recent study, where it has been clearly demonstrated that the strong adsorption of lithium superoxide on the catalyst surface retards ORR.[36]

Looking at the fractional coverage of surface by S, O_2^*, and LiO_2^* as a function of voltage (current) helps one better understand the kinetics of ORR according to the present model. The θ_s, θ_{O_2}, and θ_{LiO_2} values for the simulation results in Figure 2b are plotted in Figure 4. Surface coverage becomes independent of potential (current) for limiting cases (i.e., $\tau \rightarrow \infty$ and $\tau \rightarrow 0$). In Figure 4, the vertical blue and magenta lines represent the limiting cases $\tau \rightarrow \infty$ and $\tau \rightarrow 0$), respectively. The surface sites are saturated by lithium superoxide ($\theta_{LiO_2} = 1$) when there is negligible contribution of solution reactions in the overall ORR kinetics. However, in the cases of sufficiently fast desorption of lithium superoxide ($\tau \rightarrow 0$), there is no lithium superoxide attached to the surface ($\theta_{LiO_2} = 0$) and the surface sites are half-filled by the ad-oxygen species ($\theta_{O_2} = 0.5$). The surface coverage is potential (current) dependent for intermediate values of τ. In this case, limited occupation of surface sites by lithium superoxide leads to higher discharge potentials (Figure 4).

Recent experimental and theoretical studies report on the dominance of the discharge product by toroidal and thin-film morphologies at low and high currents, respectively.[19,21,26] Following the kinetic model set forth earlier in this study, the relative consumption rate of the lithium superoxide at the surface (i.e., film build up) and the solution (i.e, toroidal growth) given in eq 17 qualitatively suggests that the morphology of the discharge product is strongly influenced by

$$\frac{\text{toroidal}}{\text{film}} \propto \frac{r_s}{r_2} = \frac{1}{\tau}\frac{1}{k_{c2}}\exp\left(\frac{\beta_2 F}{RT}\Phi\right) \qquad (17)$$

both desorption of lithium superoxide (τ) and current (potential). Lower τ and current (high potential) are in favor of solution-mediated reactions (i.e., disproportionation), and hence, the toroidal morphology is promoted. On the other hand, the discharge product is confined to a film on the surface under high rates of discharge (low potential) and negligible desorption of lithium superoxide (high τ). Of course, the different nature of the nucleation sites on the cathode surface will also indirectly contribute to different morphologies in the nucleation and growth mechanism by affecting the desorption process at those sites.

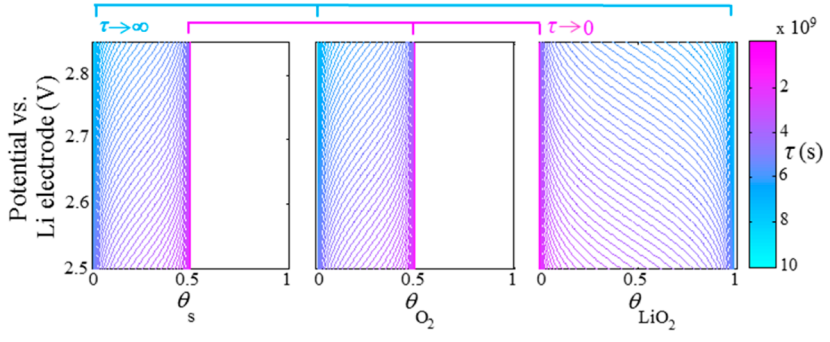

Figure 4. Simulated coverage of surface by free sites (θ_s), oxygen (θ_{O_2}), and lithium superoxide (θ_{LiO_2}) that correspond to Figure 2. τ is color-coded from dark magenta (10^{-4}) to light blue (10^{10}).

dx.doi.org/10.1021/jz5018202 | J. Phys. Chem. Lett. 2014, 5, 3486−3491

The kinetic analysis provided in this study suggests that the redistribution of lithium superoxide reactions from surface to the solution phase accounts for the unique morphological and electrochemical features reported for ORR in aprotic Li–O_2 cells. Our experimental reports of curvature in Tafel plots (in accord with those reported in the literature), along with formation of film-like products at higher currents as opposed to large toroidal agglomerates for small currents, and the presence of superoxide-like species in the final discharge products all validate the physical picture depicted for ORR in this study. On desorption from the surface, lithium superoxide will participate in both chemical disproportionation and side reactions. In both cases, apparent kinetic improvement is obtained in the form of higher discharge potentials, and one should be cautious to attribute kinetic improvements only to the effect of cathode/catalyst. We note that our treatment is general, and extends to any system where solubilization of lithium superoxide is promoted, including by solvents such as DMSO, or by phase transfer catalysts.

AUTHOR INFORMATION

Corresponding Author

*E-mail: lfnazar@uwaterloo.ca.

Notes

The authors declare no competing financial interest.

ACKNOWLEDGMENTS

We gratefully acknowledge NRCan for funding through their EcoEII program. We thank NSERC for partial financial support through their Discovery Grant and Chair programs, and B.A. acknowledges partial support of research as part of the Joint Center for Energy Storage Research, an Energy Innovation Hub funded by the U.S. Department of Energy, Office of Science, Basic Energy Sciences. We thank Charles Delacourt (Université de Picardie, France) for fruitful discussions.

REFERENCES

(1) Abraham, K. M.; Jiang, Z. A Polymer Electrolyte-Based Rechargeable Lithium/Oxygen Battery. *J. Electrochem. Soc.* **1996**, *143*, 1–5.

(2) Lei, Y.; Lu, J.; Luo, X.; Wu, T.; Du, P.; Zhang, X.; Ren, Y.; Wen, J.; Miller, D. J.; Miller, J. T.; Sun, Y.-K.; Elam, J. W.; Amine, K. Synthesis of Porous Carbon Supported Palladium Nanoparticle Catalysts by Atomic Layer Deposition: Application for Rechargeable Lithium-O_2 Battery. *Nano Lett.* **2013**, *13*, 4182–4189.

(3) Lu, Y.-C.; Shao-Horn, Y. Probing the Reaction Kinetics of the Charge Reactions of Nonaqueous Li–O_2 Batteries. *J. Phys. Chem. Lett.* **2013**, *4*, 93–99.

(4) Chen, Y.; Freunberger, S. A.; Peng, Z.; Bardé, F.; Bruce, P. G. The Li–O_2 Battery with a Dimethylformamide Electrolyte. *J. Am. Chem. Soc.* **2012**, *134*, 7952–7957.

(5) Christensen, J.; Albertus, P.; Sanchez-Carrera, R. S.; Lohmann, T.; Kozinsky, B.; Liedtke, R.; Ahmed, J.; Kojic, A. A Critical Review of Li/Air Batteries. *J. Electrochem. Soc.* **2012**, *159*, R1–R30.

(6) Garcia-Araez, N.; Novak, P. Critical Aspects in the Development of Lithium-Air Batteries. *J. Solid State Electrochem.* **2013**, *17*, 1793–1807.

(7) Hummelshøj, J. S.; Luntz, A. C.; Nørskov, J. K. Theoretical Evidence for Low Kinetic Overpotentials in Li–O_2 Electrochemistry. *J. Chem. Phys.* **2013**, *138*, 034703-(1–12).

(8) Pang, Z.; Freunberger, S. A.; Chen, Y.; Bruce, P. G. A Reversible and Higher-Rate Li–O_2 Battery. *Science* **2012**, *3*, 563–566.

(9) Cheng, F.; Chen, J. Metal–Air Batteries: From Oxygen Reduction Electrochemistry to Cathode Catalysts. *Chem. Soc. Rev.* **2012**, *41*, 2172–2192.

(10) Ramaswamy, N.; Mukerjee, S. Fundamental Mechanistic Understanding of Electrocatalysis of Oxygen Reduction on Pt and Non-Pt Surfaces: Acid versus Alkaline Media. *Adv. Phys. Chem.* **2012**, *2012*, 491604(1–17).

(11) Laoire, C. O.; Mukerjee, S.; Abraham, K. M. Elucidating the Mechanism of Oxygen Reduction for Lithium-Air Battery Applications. *J. Phys. Chem. C* **2009**, *113*, 20127–20134.

(12) Laoire, C. O.; Mukerjee, S.; Abraham, K. M. Influence of Nonaqueous Solvents on the Electrochemistry of Oxygen in the Rechargeable Lithium-Air Battery. *J. Phys. Chem. C* **2010**, *114*, 9178–9186.

(13) Lu, Y.-C.; Gasteiger, H. A.; Crumlin, E.; McGuire, R., Jr.; Shao-Horn, Y. Electrocatalytic Activity Studies of Select Metal Surfaces and Implications in Li-Air Batteries. *J. Electrochem. Soc.* **2010**, *157*, A1016–A1025.

(14) Peng, Z.; Freunberger, S. A.; Hardwick, L. J.; Chen, Y.; Giordani, V.; Barde, F.; Novak, P.; Graham, D.; Tarascon, J.-M.; Bruce, P. G. Oxygen Reactions in a Non-Aqueous Li^+ Electrolyte. *Angew. Chem. Int. Ed.* **2011**, *50*, 6351–6355.

(15) McCloskey, B. D.; Scheffler, R.; Speidel, A.; Girishkumar, G.; Luntz, A. C. On the Mechanism of Nonaqueous Li–O_2 Electrochemistry on C and Its Kinetic Overpotentials: Some Implications for Li–Air Batteries. *J. Phys. Chem. C* **2012**, *116*, 23897–23905.

(16) Gunasekara, I.; Mukerjee, S.; Plichta, E. J.; Hendrickson, M. A.; Abraham, K. M. Microelectrode Diagnostics of Lithium-Air Batteries. *J. Electrochem. Soc.* **2014**, *161*, A381–A392.

(17) Zhai, D.; Wang, H.-H.; Lau, K. C.; Gao, J.; Redfern, P. C.; Kang, F.; Li, B.; Indacochea, E.; Das, U.; Sun, H.-H.; Sun, H.-J.; Amine, K.; Curtiss, L. A. Raman Evidence for Late Stage Disproportionation in a Li–O_2 Battery. *J. Phys. Chem. Lett.* **2014**, *5*, 2705–2710.

(18) Das, U.; Lau, K. C.; Redfern, P. C.; Curtiss, L. A. Structure and Stability of Lithium Superoxide Clusters and Relevance to Li–O_2 Batteries. *J. Phys. Chem. Lett.* **2014**, *5*, 813–819.

(19) Adams, B. D.; Radtke, C.; Black, R.; Trudeau, M. L.; Zaghib, K.; Nazar, L. F. Current Density Dependence of Peroxide Formation in the Li–O_2 Battery and Its Effect on Charge. *Energy Environ. Sci.* **2013**, *6*, 1772–1778.

(20) Yang, J.; Zhai, D.; Wang, H.-H.; Lau, K. C.; Schlueter, J. A.; Du, P.; Myers, D. J.; Sun, Y.-K.; Curtiss, L. A.; Amine, K. Evidence for Lithium Superoxide-like Species in the Discharge Product of a Li–O_2 Battery. *Phys. Chem. Chem. Phys.* **2013**, *15*, 3764–3771.

(21) Zhai, D.; Wang, H.-H.; Yang, J.; Lau, K. C.; Li, K.; Amine, K.; Curtiss, L. A. Disproportionation in Li–O_2 Batteries Based on Large Surface Area Carbon Cathode. *J. Am. Chem. Soc.* **2013**, *135*, 15364–15372.

(22) Meini, S.; Piana, M.; Tsiouvaras, N.; Garsuch, A.; Gasteiger, H. A. The Effect of Water on the Discharge Capacity of a Non-Catalyzed Carbon Cathode for Li–O_2 Batteries. *Electrochem. Solid-State Lett.* **2012**, *15*, A45–A48.

(23) Mitchell, R. R.; Gallant, B. M.; Thompson, C. V.; Shao-Horn, Y. All-Carbon-Nanofiber Electrodes for High-Energy Rechargeable Li–O_2 Batteries. *Energy Environ. Sci.* **2011**, *4*, 2952–2958.

(24) Gallant, B. M.; Mitchell, R. R.; Kwabi, D. G.; Zhou, J.; Zuin, L.; Thompson, C. V.; Shao-Horn, Y. Chemical and Morphological Changes of Li–O_2 Battery Electrodes Upon Cycling. *J. Phys. Chem. C* **2012**, *116*, 20800–20805.

(25) Viswanathan, V.; Norskov, J. K.; Speidel, A.; Scheffler, R.; Gowda, S.; Luntz, A. C. Li–O_2 Kinetic Overpotentials: Tafel Plots from Experiment and First-Principles Theory. *J. Phys. Chem. Lett.* **2013**, *4*, 556–560.

(26) Horstmann, B.; Gallant, B.; Mitchell, R.; Bessler, W. G.; Shao-Horn, Y.; Bazant, M. Z. Rate-Dependent Morphology of Li_2O_2 Growth in Li–O_2 Batteries. *J. Phys. Chem. Lett.* **2013**, *4*, 4217–4222.

(27) Sharon, D.; Etacheri, V.; Garsuch, A.; Afri, M.; Frimer, A. A.; Aurbach, D. On the Challenge of Electrolyte Solutions for Li–Air Batteries: Monitoring Oxygen Reduction and Related Reactions in Polyether Solutions by Spectroscopy and EQCM. *J. Phys. Chem. Lett.* **2013**, *4*, 127–131.

(28) Gittleson, F. S.; Sekol, R. C.; Doubek, G.; Linardi, M.; Taylor, A. D. Catalyst and Electrolyte Synergy in Li−O_2 Batteries. *Phys. Chem. Chem. Phys.* **2014**, *16*, 3230−3237.
(29) Viswanathan, V.; Thygesen, K. S.; Hummelshoj, J. S.; Norskov, J. K.; Girishkumar, G.; McCloskey, B. D.; Luntz, A. C. Electrical Conductivity in Li_2O_2 and Its Role in Determining Capacity Limitations in Non-Aqueous Li−O_2 Batteries. *J. Chem. Phys.* **2011**, *135*, 214704(1−10).
(30) Albertus, P.; Girishkumar, G.; McCloskey, B. D.; Sanchez-Carrera, R. S.; Kozinsky, B.; Christensen, J.; Luntz, A. C. Identifying Capacity Limitations in the Li/Oxygen Battery Using Experiments and Modeling. *J. Electrochem. Soc.* **2011**, *158*, A343−A351.
(31) Newman, J.; Thomas-Alyea, K. E. *Electrochemical Systems*; Wiley-Interscience: Hoboken, NJ, 2004.
(32) Freunberger, S. A.; Chen, Y.; Peng, Z.; Griffin, J. M.; Hardwick, L. J.; Barde, F.; Novak, P.; Bruce, P. G. Reactions in the Rechargeable Lithium−O_2 Battery with Alkyl Carbonate Electrolytes. *J. Am. Chem. Soc.* **2011**, *133*, 8040−8047.
(33) Herranz, J.; Garsuch, A.; Gasteiger, H. A. Using Rotating Ring Disc Electrode Voltammetry to Quantify the Superoxide Radical Stability of Aprotic Li−Air Battery Electrolytes. *J. Phys. Chem. C* **2012**, *116*, 19084−19094.
(34) Thotiyl, M.M. O.; Frendberger, S. A.; Peng, Z.; Chen, Y.; Liu, Y.; Bruce, P. G. A Stable Cathode for the Aprotic Li−O_2 Battery. *Nat. Mater.* **2013**, *12*, 1050−1056.
(35) Holewinski, A.; Linic, S. J. Elementary Mechanisms in Electrocatalysis: Revisiting the ORR Tafel Slope. *Electrochem. Soc.* **2012**, *159*, H864−H870.
(36) Choi, R.; Jung, J.; Kim, G.; Song, K.; Kim, Y. I.; Jung, S. C.; Han, Y.-K.; Song, H.; Kang, Y.-M. Ultra-Low Overpotential and High Rate Capability in Li−O_2 Batteries Through Surface Atom Arrangement of PdCu Nanocatalysts. *Energy Environ. Sci.* **2014**, *7*, 1362−1368.